Accelerated crystallization of zeolites via hydroxyl free radicals

Guodong Feng,[1†] Peng Cheng,[1†]Wenfu Yan,[1]Mercedes Boronat,[3]Xu Li,[1]Jihu Su,[2]Jianyu Wang,[1]Yi Li,[1]Avellino Corma,[3]Ruren Xu,[1]Jihong Yu[1*]

[1]State Key Laboratory of Inorganic Synthesis and Preparative Chemistry, College of Chemistry, Jilin University, 2699 Qianjin Street, Changchun, 130012, P. R. China

[2]Hefei National Laboratory for Physical Sciences at Microscale and Department of Modern Physics, University of Science and Technology of China, ~~No.~~96~~,~~ JinZhai Road, Hefei, 230026, P. R. China

[3]Instituto de TecnologiaQuimica, Universidad Politecnica de Valencia, Consejo Superior de InvestigacionesCientificas ~~(UPV-CSIC)~~, Valencia, 46022, Spain

***Corresponding author. E-mail: jihong@jlu.edu.cn**

†These authors contributed equally to this work.

In the hydrothermal crystallization of zeolites from basic media, hydroxide ions (OH^-) catalyze the depolymerization of the aluminosilicate gel by breaking the Si,Al-O-Si,Al bonds and the polymerization of the aluminosilicate anions around the hydrated cation species, by remaking the Si,Al-O-Si,Al bonds. We report that hydroxyl free radicals (•OH) are involved in the zeolite crystallization under hydrothermal conditions. The crystallization processes of zeolites, such as Na-A ~~(LTA)~~, Na-X ~~(FAU)~~, NaZ-21 ~~(LTN)~~, and Silicalite-1 ~~(MFI)~~, can be accelerated ~~by about a factor of 2~~ with hydroxyl free radicals generated by ultraviolet irradiation or Fenton reagent.

One Sentence Summary: The •OH free radicals were found to be involved in the hydrothermal synthesis of zeolites and can remarkably accelerate their crystallization process.

Zeolites are microporous crystalline aluminosilicates ~~with compensating cations of group IA and IIA elements, such as sodium, potassium, magnesium, and calcium~~ that are used as ion-exchangers in

Código de campo cambiado

Con formato: Español (alfab. internacional)

Con formato: Español (alfab. internacional)

detergent industry, catalysts in petrochemical and chemical industry, and adsorbents in air separation by pressure swing adsorption(*1, 2*). Zeolite materials are typically synthesized in a strong basic medium in which a high concentration of hydroxide ions (OH^-) assists in the mineralization of silicate and aluminate species in the reactant gels(*3*). The crystallization process can be described through the following steps: i) polymerization forming an amorphous gel via making Si,Al-O-Si,Al bonds, ii) depolymerization forming soluble aluminosilicates and silicates via breaking Si,Al-O-Si,Al bonds, and iii) re-polymerization remaking Si,Al-O-Si,Al bonds around the hydrated cation species, that is, the structure-directing agents, via condensation reaction(*4, 5*). These steps comprise the nucleation and crystal growth stage of the crystallization, which are catalyzed by OH^- involving multiple equilibria. However, the crystallization mechanism of zeolites is still unclear and the understanding of their formation at molecular level has not been achieved yet.

Under basic conditions, OH^- ions increase the coordination of tetrahedral Si atoms to pentahedral or octahedral, which weaken and break the Si-O-Si bonds(*6*). ~~However~~Notably, theoretical calculations show that the dissociation of the Si-O-Si bonds is more favorable when catalyzed by hydroxyl free radicals(•OH)(*7, 8*); •OH species are highly active in organic synthesis (*9*), polymerization (*10*), and modification of proteins (*11*). Generation of •OH in solution can be achieved by electron pulse radiolysis, ~~ultraviolet (~~UV~~)~~irradiation, Fenton reactions, chemical reactions, and high-voltage electrical discharge, etc (*11*). We show that hydrothermal zeolite crystallization can be accelerated by introducing •OH ~~hydroxyl free radicals~~ via physical or chemical methods.

To investigate the effect of •OH on ~~the~~ zeolite crystallization, a modified multiparallel reactor was used that allowed for UV irradiation and controlled heating (fig. S1). The hydrothermal syntheses

conducted under UV irradiation are referred to as UV condition, and control syntheses conducted in the oven without the UV irradiation are referred to as dark condition. We initially studied the UV and dark-condition syntheses in the Na_2O-Al_2O_3-SiO_2-H_2O system at298 K. Under UV conditions for 24 h, the experimental and simulated ~~x~~X-ray diffraction (XRD) patterns of Na-X (SiO_2/0.21Al_2O_3/9.36Na_2O/85H_2O, ~~LTA,~~ Fig 1A), NaZ-21(SiO_2/0.32Al_2O_3/10.05Na_2O/85H_2O**,** ~~LTN~~ Fig 1B), and Na-A (SiO_2/0.46Al_2O_3/4.4Na_2O/60H_2O,~~LTA,~~ fig. S2A), and the SEM images of the corresponding products (fig.S3) indicate that the products were already crystallized. Under dark conditions for 24 hours, the corresponding XRD patterns (Fig. 1, C and D and fig. S2B),show that the materials were still primarily amorphous. These results demonstrate that the crystallization rate of zeolites was accelerated by UV irradiation.

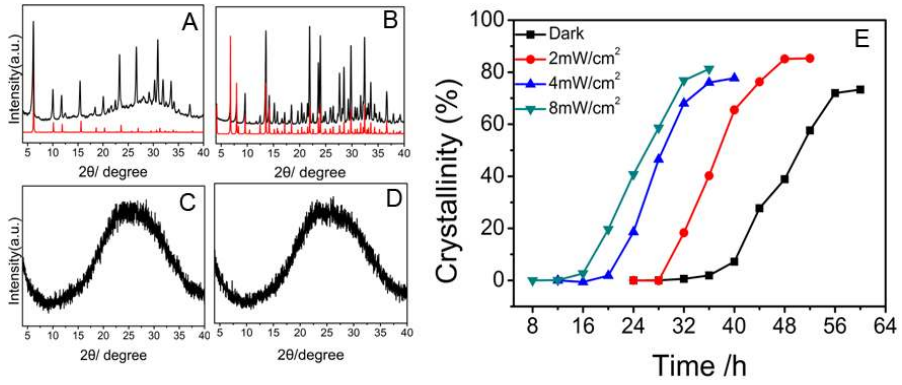

Fig. 1.Crystallization processes under UV irradiation and dark conditions at 298 K. ~~**(A to D)**~~ The experimental XRD patterns of Na-X and NaZ-21synthesized under the UV conditions (**A and B,** black, 4.0 mW/cm^2) and dark conditions (**C and D,** black) for 24 h, respectively. The corresponding simulated XRD patterns are plotted for comparison (**A and B,** red). Crystallization curves of zeolite Na-A (**E**) under dark conditions and under UV conditions with irradiance of 2.0, 4.0, and 8.0mW/cm^{2}with a Na_2O/SiO_2 ratio of 4.4.The crystallinity is defined as the ratio of the integrated intensity of the two most intense peaks (2θ= 23.96° and 29.92°) of the sample respect to a well-crystallized standard sample.

The crystallization process of zeolite Na-A with the starting molar composition of SiO_2: $0.46Al_2O_3$: $4.4Na_2O$: $60H_2O$was further investigated at 298 K under dark and UV conditions with different irradiances that varied the •OH concentration (reported as crystallization curves in Fig 1E). Under dark conditions, long-range ordering of zeolite Na-A, as confirmed by XRD, began to be observed after40h (fig. S4A). After 60 h, highly crystalline zeolite Na-A was obtained, as confirmed by the SEM and HRTEM images (fig. S5). In contrast, the XRD patterns (fig. S4B, C, D)) show that the long-range ordering of zeolite Na-A was already observed at 32, 20, and 16h and highly crystalline zeolite A was obtained at 52, 40, and 36hfor irradiances of 2.0, 4.0, and 8.0 mW/cm^2,respectively as shown in the SEM and TEM images (fig. S6-S8).

Reducing the OH^- concentration could slow down the crystallization of zeolites. We further studied the crystallization behavior of the initial reaction mixture with a reduced Na_2O/SiO_2 molar ratio[3.08 vs 4.4]at 298 K. Under the dark conditions, the long-range ordering of zeolite Na-A was not observed until45h and the crystals have been well-developed when the reaction time reached 55 h (fig. S9A: XRD; fig. S10: SEM and TEM images), while long-range ordering was already observed at 40h when the Na_2O/SiO_2 ratio was 4.4 (fig. S4A). In contrast, when the initial reaction mixture was irradiated with UV lamp, highly-crystalline Na-A was formed at 40 h (fig. S9B: XRD; fig. S11: SEM and TEM images). The results presented above clearly demonstrate that reducing OH^- decreases the crystallization rate of zeolite; whereas •OH can promote the crystallization at the same time. Consequently, the crystallization rate of zeolite Na-A under UV with Na_2O/SiO_2 ratio of 3.08 is even faster than that under dark with Na_2O/SiO_2 ratio of 4.4. Notably, the accelerating effect on crystallization upon UV with the reduced alkalinity is further enhanced compared to that upon UV

with normal alkalinity.

Upon UV irradiation, water can generate •OH(*11*).We used electron paramagnetic resonance (EPR) to characterize •OH and the derived species formed in the zeolite reaction system. 5,5-dimethylpyrroline-*N*-oxide (DMPO) as the spin-trapping agent of •OH was added ~~as the spin trapping agent of •OH~~ into the initial reaction mixture, and the EPR signals were recorded in situ after the reaction mixture was irradiated for 0, 30~~,~~ and 90 s. For comparison, the initial reaction mixture and the pure water were also characterized under dark conditions. As anticipated, the EPR signals from •OH captured by the DMPO, i.e., a 1:2:2:1 quartet pattern with a splitting of 15.0 G characteristic of a DMPO-$^{\bullet}$OH adduct, were observed after irradiation for 90 s (Fig 2A) and 30 s (Fig. 2B). ~~because~~ Because DMPO ~~is~~ was also photolyzed, the EPR signals of oxidized DMPO radicals featured by a three-line spectrum were also observed~~)~~. Strikingly, sextet EPR signals (Fig. 2, Aand B) with large hyperfine coupling constant (a_N: 1.59 mT, a^{β}_{Hr}: 4.5 mT) were observed. None of these signals were observed in the spectrum of the initial reaction mixture without the UV irradiation (0 s) in the presence of ~~the spin trapping agent~~ DMPO (Fig. 2C), indicating that the new sextet EPR signals were not from the inorganic impurities of the initial reaction mixture but from the radicals generated by the UV irradiation.

Because of the large hyperfine coupling constant, these sextet EPR signals cannot be attributed to the carbon- (C) and oxygen- (O) centered radicals. ~~The value of a^{β}_{Hr} could be used to characterize the radical species.~~ For the carbon-centered radical, the a^{β}_{Hr} is at the range of 1.8 to2.8 mT; and the oxygen-centered radical, the a^{β}_{Hr} is at the range of 0.7 to1.4 mT (*12, 13*). In ~~addition~~fact, the large hyperfine coupling constant of these sextet EPR signals is similar to that of the DMPO-$^{\bullet}$P(O)$(OC_2H_5)_2$

adduct (*12*). Because no P species was involved in the initial reaction mixture, these signals might be attributed to the DMPO-˙Si adduct. If this is so, then the slight change in the intensity of these signals in the spectra after 30 and 90 s of irradiation ~~suggested~~ indicated that these Si-based radicals were generated during the zeolite crystallization.

Previous studies show that fumed silica has an intrinsic population of planar three-membered-rings (3MRs) formed at high temperature and 'frozen-in' by rapid quenching, that can undergo cleavage forming Si• and Si-O• radicals because of the strain in the Si-O-Si bonds (*14-16*). Aqueous alkaline silicate solutions also contain 3MRs, as confirmed by previous ^{29}Si–^{29}Si COSY NMR studies(*17*). Thus, the silicon-based radicals in zeolite synthesis probably form through homolytic cleavage of the strained Si-O-Si bonds in planar 3MRs in the initial reaction mixture. The reason why no Si-O• radicals were observed might be caused by their high activity; they can easily react with water to form •OH. Fig. 2, D to F, show the comparison of the experimental and the simulated EPR spectra of DMPO-˙OH adduct, DMPO-˙Si adduct, and oxidized DMPO radicals, respectively, that confirms the assignment.

Considering that the concentration of radicals in the non-UV irradiated initial reaction mixture and in the pure water might be too low to be detected by DMPO, a recently developed spin-trapping agent, 5-tert-butoxycarbonyl-5-methyl-1-pyrroline-*N*-oxide (BMPO) was used, that allows a long time accumulation of the EPR signals(*18*). Strikingly, •OH ~~was~~ was also observed ~~-~~in the initial synthesis mixture under dark conditions for 10 h (Fig. 2(G)). The EPR signals arose from •OH-captured by BMPO, i.e., a characteristic 1:2:2:1 quartet pattern of a BMPO-˙OH adduct, were recorded (*18*). Pure water under dark conditions did not give any EPR signals (fig. S12), suggesting that •OH came from

the zeolite reaction system. The observation of •OH in the initial mixture under dark conditions suggests that, in addition to OH^-,•OH was also involved in the zeolite crystallization as mineralizers. Although the reactivity of the •OH is much greater than that of OH^-, the concentration difference favors the OH^- mechanism.

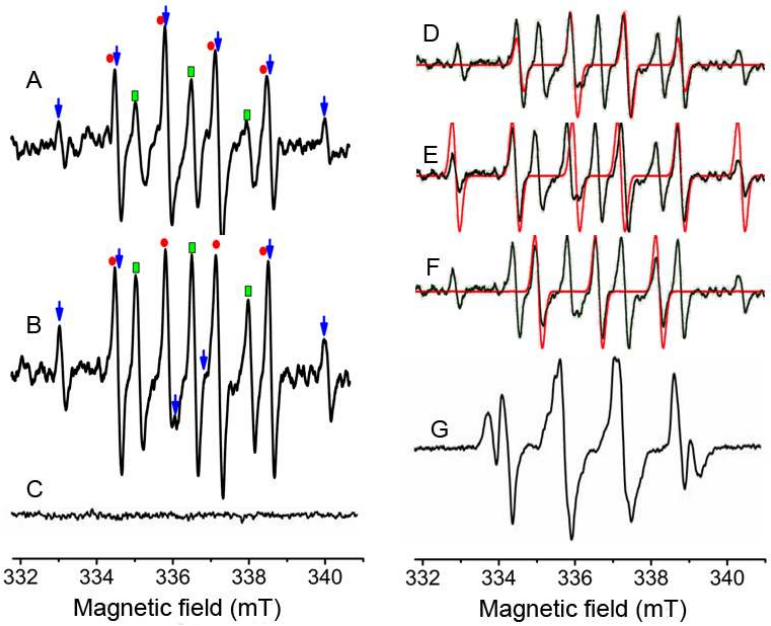

Fig. 2. Radicals' identification from UV irradiation. EPR spectra of the initial reaction mixture containing the spin-trapping agent of DMPO under the UV irradiation for(**A**) 90 s, (**B**)30 s, and (**C**) 0 s, comparison of the experimental and the simulated EPR spectra of DMPO-•OH adduct (**D**), DMPO-•Si adduct (**E**), and oxidized DMPO radicals (**F**). EPR spectrum of the initial reaction mixture containing the spin-trapping agent of BMPO (**G**) under dark conditions. The EPR signals are marked as following: hydroxyl free radicals (●); oxidized DMPO radicals (▮);silicon-based radicals (🡻).

The Fenton reagent can also produce •OH, and we investigated the crystallization process for ~~silicalite~~Silicalite-1 in the reaction system TPAOH-TEOS-H_2O with the addition of the Fenton reagent(9TPAOH/25SiO_2/480H_2O/100EtOH/0.015H_2O_2/0.001$FeSO_4$•18H_2O, 343 K). The XRD

patterns of the solid products (Fig.3A) indicate that the long-rang ordering of Silicalite-1 was already observed when the reaction time reached 40 h, which is 10 h shorter than that under UV conditions (Fig 3B) and 20 hours shorter than under dark conditions (Fig. 3C). The greater acceleration effect of the Fenton conditions than UV conditions indicates the higher concentration of •OH generated by the Fenton reagent than by the UV irradiation. Fig. S13 shows the SEM and TEM images of Silicalite-1 recovered at the end of crystallization under Fenton conditions as compared with the dark and UV conditions. Fig. S14 gives the yields of Silicalite-1 at different crystallization periods under Fenton conditions, which are also remarkably improved compared to the dark conditions. The composition and N_2 adsorption data for all samples are included in table S1.

To identify the radicals in the crystallization of Silicalite-1,the initial reaction mixtures at ambient temperature under Fenton, UV, and dark conditions were characterized by EPR spectroscopy (Fig.3, D to F). Under dark conditions, signals from the BMPO-$^{\bullet}CH(CH_3)OH$ adduct (Fig. 3F, a_N: 1.51 mT, a_H: 2.1 mT) imply the existence of alkane radicals, which may be formed from the reaction of •OH with the ethanol generated from the hydrolysis of TEOS. This reaction would consume of the very limited •OH formed under the dark conditions. Under UV conditions, DMPO-$^{\bullet}CH(CH_3)OH$(a_N: 1.59 mT, a^{β}_H: 2.27 mT), DMPO-$^{\bullet}OH$ (a_N: 1.50 mT, a^{β}_H: 1.50 mT), DMPO-$^{\bullet}Si$ (a_{other}: 4.5 mT), and oxidized DMPO radicals were observed and indicate that more •OH formed. The initial reaction mixture under the Fenton conditions (Fig. 3D) contained •OH ~~radicals~~ (Fig.3E;a_N: 1.50 mT, a^{β}_H: 1.50 mT), ethanol carbon radicals (a_N: 1.59 mT, a^{β}_H: 2.27 mT), silicon-based radicals, a_{other}: 4.5 mT), and oxidized DMPO radicals.

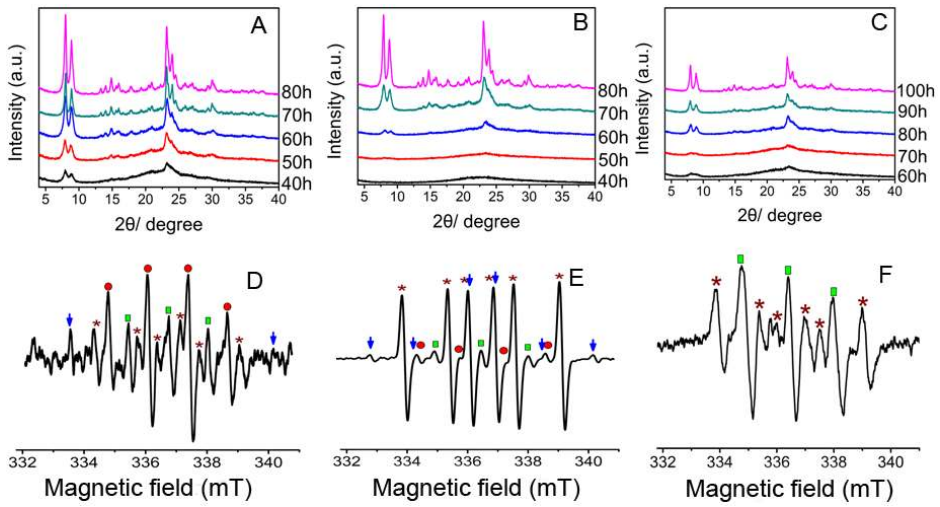

Fig. 3.Acceleration processes by Fenton reagent. Crystallization processes of Silicalite-1 at 343 K under(**A**) Fenton conditions (**B**), UV conditions (4.0mW/cm^2) and (**C**) dark conditions, EPR spectra of the TPAOH-TEOS-H_2O system under (**D**) Fenton conditions (**E**), UV conditions (4.0mW/cm^2) and (**F**) dark conditions. The EPR signals are marked as following:•OH(●);oxidized BMPO radicals(■); oxidized DMPO radicals (■); silicon-based radicals (🡻); ethanol radicals (*).

Inhibiting •OH may slow down the zeolite crystallization. Because ethanol is an effective •OH scavenger, we crystallized Silicalite-1 at 343 K under UV conditions by evaporating the ethanol in the mixture. Two batches of the initial mixtures with the same molar composition were prepared, which were stirred overnight at ambient temperature under dark conditions in sealed and open quartz tubes, respectively. The weight loss of the initial mixture in the open quartz tube suggests that most of the ethanol hydrolyzed from TEOS was evaporated from the mixture. Subsequently, the quartz tubes were surely sealed and heated at 343 K for 48 h under UV irradiation. As anticipated, the crystallization process was accelerated when the ethanol was removed as indicated by the corresponding XRD patterns (fig. S15).

The zeolite crystallization is a two-step process including ~~seed formation (~~nucleation~~)~~ and ~~growth of the stable seed (~~crystal growth~~)~~. The sigmoidal crystallization curves shown in Fig. 1Eshow that the induction period under UV conditions is much shorter than that under dark conditions, which suggests that •OH generated by UV irradiation plays an important role in accelerating the nucleation stage during the crystallization. However, the slope of the crystallization curve for the UV conditions is similar to that for the dark conditions, implying similar crystal growth rates. To further confirm which stage was accelerated by •OH, we investigated the synthesis of zeolite Na-A at 298 K by UV pretreatment in the induction period for 18 h followed by crystallization under dark conditions. The XRD patterns of the products (fig. S16) show that the crystallization of the synthetic system under such conditions is similar to that under UV conditions, indicating that •OH mostly influences the nucleation stage but not the crystal growth stage. ~~In the nucleation stage, the de-polymerization of the aluminosilicate gel by breaking the Si,Al-O-Si,Al bonds and the polymerization of the aluminosilicate anions around the hydrated cation speciesby remaking the Si,Al-O-Si,Al bonds will happen.~~

Theoretical calculations provide more insight into how •OH accelerates the nucleation stage. ~~All calculations were performed using the B3LYP functional and the 6-311+G(d,p) basis set as implemented in the Gaussian09 software package(*19-22*). Geometries were fully optimized without restrictions, and the nature of the stationary points was characterized by means of frequency calculations. Electronic energies (E) and Gibbs free energies (G) were computed for all structures and processes.~~

We first considered the depolymerization of the gel by breaking of the Si-O-Si bonds under very basic conditions. The reaction electronic energies ΔE and Gibbs free energies ΔG that are always

clearly exothermic indicate that under such basic media the $[Si_2O_{1+x}(OH)_{6-x}]Na_x$ species will be preferentially formed. The synthesis was carried out under very basic conditions, we studied the thermodynamics of successive deprotonation steps and stabilization of the anionic $[Si_2O_{1+x}(OH)_{6-x}]^{x-}$ species with Na^+ cations generating neutral $[Si_2O_{1+x}(OH)_{6-x}]Na_x$ species via successive deprotonation steps (fig. S17). The reaction of a dimeric silicon species with NaOH results in deprotonation of the silicon unit generating an anionic species stabilized with Na^+ plus water. The reaction electronic energies ΔE and Gibbs free energies ΔG are always clearly exothermic, indicating that under such basic media the negatively charged silicates stabilized by Na^+ cations will be preferentially formed.

Con formato: Sin Resaltar

Con formato: Resaltar

We next studied the attack of either OH^- or •OHto the model of the gel in a highly deprotonated $[SiO_2(OH)\text{-}O\text{-}SiO_3]Na_5$ system(Fig. 4A). Water reacts with the dimeric silicon species through TS1 forming a pentacoordinated intermediate I1, with an activation barrier of only 10 kcal/mol (see profile in Fig. 4C-blue line). Then, there is an additional H transfer step that converts intermediate I1 into intermediate I2 with an activation barrier of only 4 kcal/mol. This intermediate rapidly dissociates into the highly stable products P through TS3 with an almost negligible activation barrier lower than 2 kcal/mol.

Similar structures are involved in the reaction of the $[SiO_2(OH)\text{-}O\text{-}SiO_3]Na_5$ model with a •OH, as shown in Fig. 4B. A H transfer step converting intermediate I1 into intermediate I2 is also necessary to have one OH group on each Si atom, which facilitates the dissociation of the Si-O bond. However, in Fig. 4C-orange line, the energies involved in the reaction with •OH are much lower than those involved in the reaction with OH^-. All the activation barriers involved in this process are lower than

1.5 kcal/mol, indicating that the presence of •OH in the reaction medium will considerably increase the rate of Si-O bond breaking and depolymerization of the gel.

The second step in the global process is the formation of new Si-O-Si ~~(or Si-O-Al)~~ bonds~~. We could~~, that could be consider~~this~~ed as the reverse process ~~already~~ above investigated, ~~and we could approximate the activation barriers for the condensation step as the highest activation energy in the reverse profile,~~ starting from products P and ending with reactants R. In the gel with $[SiO_2(OH)\text{-}O\text{-}SiO_3]Na_5$ model, the high stability of the products results in very high activation energies, 30 kcal/mol in the presence of only OH^-, and somewhat lower, 23 kcal/mol, when •OH ~~was~~ is also present in the media.

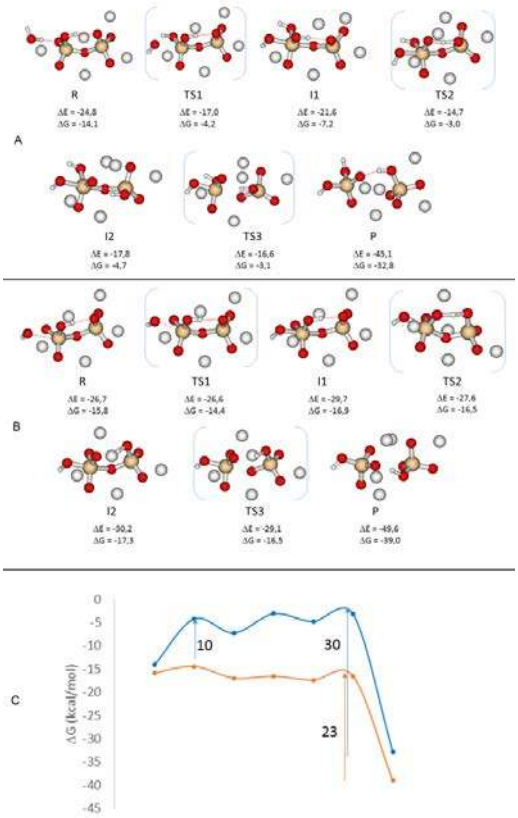

Fig. 4.Reaction of $[SiO_2(OH)\text{-}O\text{-}SiO_3]Na_5$ system and Gibbs free energy calculation. Reaction of $[SiO_2(OH)\text{-}O\text{-}SiO_3]Na_5$ system with (**A**) OH^- and with (**B**) •OH. Calculated Gibbs free energy profiles for the reaction of $[SiO_2(OH)\text{-}O\text{-}SiO_3]Na_5$ model with OH^-(blue) and with •OH (orange) (C).Electronic (ΔE) and Gibbs free energies (ΔG) are given in kcal/mol.

We also considered the reaction of monodeprotonated $[Si(OH)_2\text{-}O\text{-}Si(OH)_3]Na$ system~~, in order to check the influence of decreased alkalinity on the breaking of the Si-O-Si bonds and the forming of new Si-O-Si bonds.~~ and the calculation results clearly prove the enhanced positive effect of •OH as compared with OH^- in breaking of the Si-O-Si bonds (activation barrier: 29 vs 4 kcal/mol) and promoting the formation of new Si-O-Si bonds (activation barrier: 17 vs 8 kcal/mol) in the gel with reduced alkalinity (fig. S18, S19). This is consistent with our experimental results of the enhanced

accelerating effect upon UV with reduced alkalinity.

In summary,

~~As shown in fig. S18, the reaction of OH^- with the dimeric $[Si(OH)_2\text{-}O\text{-}Si(OH)_3]Na$ species results in proton abstraction forming water in a barrierless exothermic process. Again, water dissociation through transition state TS1 yields a pentacoordinated intermediate with an activation energy of 29 kcal/mol, which subsequently decomposes to the monomeric species via transition state TS2 with an activation barrier of only 5 kcal/mol. There is however an increase in the reactivity with •OH. The barrier for the first step of the mechanism decreases to 4 kcal/mol (fig. S19).~~

~~For the second step in the formation of new Si-O-Si (or Si-O-Al) bonds, we obtain values of 17 and8 kcal/mol for the reaction of monodeprotonated $[Si(OH)_2\text{-}O\text{-}Si(OH)_3]Na$ system in the presence of hydroxide anions and presence of •OH, respectively. These values would clearly prove the enhanced positive effect of the hydroxyl free radicals in promoting the formation of new Si-O-Si (or Si-O-Al) bonds in the gel with reduced alkalinity. This is also consistent with our experimental results that the accelerating effect upon UV in the reduced alkalinity was enhanced.~~

~~Recently, Yeong and coworkers reported the accelerated synthesis of deca-dodecasil 3rhombohedral (DDR3) zeolite crystals via hydrothermal growth coupled with ultrasonic irradiation method(*23*). Compared to the conventional hydrothermal synthesis at 433 K, the synthesis duration of DDR3 zeolite crystals was reduced from 25 days to 1 day. It is believed that this is mainly due to the role of the free radicals produced by the ultrasonic energy that helps for the rapid nucleation of zeolite materials.~~

~~T~~the discovery that zeolite synthesis mechanism can be promoted through free radicals sheds a

Con formato: Inglés (Reino Unido)

new light on zeolite crystallization, and will open~~s~~ new perspectives for ~~energy efficient~~ the synthesis of zeolite materials that are largely demanded in chemical industry.

REFERENCES AND NOTES

1. Y. Li, J. H. Yu, New Stories of Zeolite Structures: Their Descriptions, Determinations, Predictions, and Evaluations. *Chem. Rev.* **114**, 7268 (2014).
2. J. Cejka *et al.*, *Zeolites and Catalysis-Synthesis, Reactions and Applications*. (WILEY-VCH Verlag GmbH & Co. KGaA, Weinheim, 2010).
3. C. S. Cundy, P. A. Cox, The Hydrothermal Synthesis of Zeolites: History and Development from the Earliest Days to the Present Time. *Chem. Rev.* **103**, 663 (2003).
4. C. S. Cundy, P. A. Cox, The hydrothermal synthesis of zeolites: Precursors, intermediates and reaction mechanism. *Micropor. Mesopor. Mat.* **82**, 1 (2005).
5. A. I. Lupulescu, J. D. Rimer, In situ imaging of silicalite-1 surface growth reveals the mechanism of crystallization. *Science* **344**, 729 (2014).
6. R. K. Iler, *The Chemistry of Silica*. Solubility, Polymerization, Colloid and Surface Properties, and Biochemistry (John Wiley & Sons, Inc, 1979).
7. Y. T. Xiao, A. C. Lasaga, Ab initio quantum mechanical studies of the kinetics and mechanisms of quartz dissolution: OH^- catalysis. *Geochim. Cosmochim. Ac.* **60**, 2283 (1996).
8. R. Konecny, Reactivity of Hydroxyl Radicals on Hydroxylated Quartz Surface. 1. Cluster Model Calculations. *J. Phys. Chem. B* **105**, 6221 (2001).
9. S. Z. Zard, *Radical reactions in organic synthesis*. (Oxford University Press, New York, 2003).
10. G. Moad, D. H. Solomon, *The chemistry of radical polymerization*. second fully revised edition (Elsevier, New York, 2006).
11. G. Z. Xu, M. R. Chance, Hydroxyl Radical-Mediated Modification of Proteins as Probes for Structural Proteomics. *Chem. Rev.* **107**, 3514 (2007).
12. G. R. Buettner, Spin trapping: ESR paramaters of spin adducts. *Free. Radical. Bio. Med.* **3**, 259 (1987).
13. A. Angelo, M. Dante, *Spin Trapping*. In Electron Paramagnetic Resonance (John Wiley & Sons, Inc., 2008), vol. 4, pp. 285-324.
14. D. L. Griscom *et al.*, ESR studies of irradiated $^{17}O^-$ enriched sol-gel silicas: Organic impurity effects and the structure of the nonbridging-oxygen hole center. *J. Non-Cryst. Solids.* **92**, 295 (1987).
15. H. Zhang *et al.*, Processing pathway dependence of amorphous silica nanoparticle toxicity: colloidal vs pyrolytic. *J. Am. Chem. Soc.* **134**, 15790 (2012).
16. W. L. Warren *et al.*, Experimental evidence for two fundamentally different E' precursors in amorphous silicon dioxide. *J. Non-Cryst. Solids.* **136**, 151 (1991).
17. C. T. G. Knight *et al.*, The structure of silicate anions in aqueous alkaline solutions. *Angew. Chem. Int. Ed.* **46**, 8148 (2007).
18. C. H. Huang, B. Z. Zhu, The first purification and unequivocal characterization of the radical form

of the carbon-centered quinone ketoxy radical adduct. *Chem. Commun.* **49**, 6436 (2013).

19. M. J. Frisch *et al.*, *Gaussian 09*. revision C.01 (Gaussian, Inc, Wallingford, CT, 2009).
20. A. D. Becke, Density - functional thermochemistry. III. The role of exact exchange. *J. Chem. Phys.* **98**, 5648 (1993).
21. G. A. Petersson, M. A. Al-Laham, A complete basis set model chemistry. II. Open - shell systems and the total energies of the first - row atoms. *J. Chem. Phys.* **94**, 6081 (1991).
22. J. Tirado-Rives, W. L. Jorgensen, Performance of B3LYP Density Functional Methods for a Large Set of Organic Molecules. *J. Chem. Theory. Comput.* **4**, 297 (2008).
23. M. Mubashir *et al.*, Accelerated synthesis of deca-dodecasil 3 rhombohedral (DDR3) zeolite crystals via hydrothermal growth coupled with ultrasonic irradiation method. *RSC Adv.* **5**, 22658 (2015).

ACKNOWLEDGMENTS

This work was supported by the the State Basic Research Project of China (2011CB808703 and 2014CB931802), National Natural Science Foundation of China (21320102001 91122029,21171063, and 21571075), and the Major International Joint Research Project of China for financial support (21320102001).W.Y. acknowledges support from the Excellent Young Scientists Fund (21222103), and the 973 Project of China (2014CB931802).
A.C. thanks the Program Severo Ochoa for financial support. We also tThank G. Li and M. Fan for experimental assistance in EPR analysesmeasurements, and J. Di, D. Xi, T. Lu for experimental assistance in zeolite synthesis.
Author contributions: J.Y. designed and supervised the project; W.Y., A.C. and R.X. involved the design of the experiments; G.F., P.C., and J. W. performed the experiments; J.S. performed the EPR analyses; M.B., X.L., and Y.L. contributed to the calculations; J.Y. and W.Y. analyzed the data; together with W.Y., A.C., R.X. and W.Y. involved the design of the experiments; G.F., P.C., and J. W. performed the experiments; J.S. performed the EPR analyses; M.B., X.L., and Y.L. contributed to the DFT calculations; G.F. made wrote the first draft; W.Y. rewrote the manuscript; J.Y. and W.Y. deeply revised the manuscript.

Supporting Online Material

Materials and Methods

Figs. S1 to S19

Table S1